

MULTI-WAVELENGTH PROPERTIES OF BARRED GALAXIES IN THE LOCAL UNIVERSE. I: VIRGO CLUSTER

LEA GIORDANO¹, KIM-VY H. TRAN^{1,2}, BEN MOORE¹ & AMÉLIE SAINTONGE^{3,4}

Draft version October 5, 2018

ABSTRACT

We study in detail how the barred galaxy fraction varies as a function of luminosity, HI gas mass, morphology and color in the Virgo cluster in order to provide a well defined, statistically robust measurement of the bar fraction in the local universe spanning a wide range in luminosity (factor of ~ 100) and HI gas mass. We combine multiple public data-sets (UKIDSS near-infrared imaging, ALFALFA HI gas masses, GOLDMine photometry). After excluding highly inclined systems, we define three samples where galaxies are selected by their B-band luminosity, H-band luminosity, and HI gas mass. We visually assign bars using the high resolution H-band imaging from UKIDSS. When all morphologies are included, the barred fraction is $\sim 17 - 24\%$ while for morphologically selected discs, we find that the barred fraction in Virgo is $\sim 29 - 34\%$: it does not depend strongly on how the sample is defined and does not show variations with luminosity or HI gas mass. The barred fraction depends most strongly on the morphological composition of the sample: when the disc populations are separated into lenticulars ($S0-S0/a$), early-type spirals ($Sa-Sb$), and late-type spirals ($Sbc-Sm$), we find that the early-type spirals have a higher barred fraction ($\sim 45 - 50\%$) compared to the lenticulars and late-type spirals ($\sim 22 - 36\%$). This difference may be due to the higher baryon fraction of early-type discs which makes them more susceptible to bar instabilities. We do not find any evidence of barred galaxies being preferentially blue.

Subject headings: galaxies:barred galaxies

1. INTRODUCTION

Instabilities in disc galaxies play an important role as these galaxies evolve through cosmic time. Secular and transient instabilities can strongly affect star formation histories, disc scale lengths, morphologies, fueling rates of central AGN etc. The bar instability is one of the most common secular effects which is observed in about two thirds of disc galaxies in the near infrared (Eskridge et al. 2000, hereafter E00). On scales smaller than 1 kpc, more than half of disc galaxies host secondary bars, central star clusters, spiral-like dust lanes, or star-forming rings (Carollo et al. 1997, 1998; Martini & Pogge 1999; Laine et al. 1999; Böker et al. 2003). Bars themselves are unstable and they can buckle to form boxy/peanut shaped bulges, similar to observed in our own Milky Way (Combes et al. 1990; Pfenniger & Norman 1990; Bureau & Athanassoula 2005; Athanassoula 2005; Martinez-Valpuesta et al. 2006; Debattista et al. 2006).

According to recent studies (van den Bergh 2002; Barazza et al. 2009), the bar fraction does not change within different environments but depends solely on host-galaxy properties. Barazza et al. (2009) finds a small increase in bar fraction only in dense central cores of clusters even though on average the fractions are comparable: $\sim 30\%$ in clusters and in the field.

In addition, there is no significant difference between

the global properties of barred and unbarred galaxies (Kaloghlian & Kandalian 1998): for a given circular velocity, they have comparable luminosities, scale lengths, colors, and star formation rates (Courteau et al. 2003). This suggests that barred and unbarred galaxies are members of the same family and do not originate from different evolutionary trees. Their structural similarity may be understood if bars are generated by transient dynamical processes that are independent of the initial galaxy formation conditions.

The main difficulty in comparing bar fractions in different environments and at different redshifts is that, depending on the inclination, the dust content and the color of the host galaxy, the bar structure in the disc can be hidden at optical wavelengths.

The first statistically robust study that looked into the difference between optical and near-infrared (NIR hereafter) bar fraction has been made by E00. Starting from an optically selected, magnitude limited ($B \leq 12$) sample (the OSU Bright Spiral Galaxy survey, Eskridge et al. 2002), including only big (diameter $D \geq 6'$) lenticular and spiral galaxies (with Hubble type $T \geq 0$) in the RC3 (de Vaucouleurs et al. 1991), they found that the NIR bar fraction is at least double than the optical one. This leads to the conclusion that RC3 bar types should be used with caution (see also Marinova & Jogee 2007).

It is interesting to note that recent studies such as Marinova & Jogee (2007); Menéndez-Delmestre et al. (2007); Barazza et al. (2008); Aguerri et al. (2009); Marinova et al. (2009) have found, for local samples of spiral galaxies, optical bar fractions as high as 70% (in case of disc dominated systems). Thus the true bar fraction could be even higher if is measured in NIR.

The variation in bar fraction statistics in previous stud-

Electronic address: giordano@physik.uzh.ch

¹ Institute for Theoretical Physics, University of Zürich, Switzerland

² George P. and Cynthia W. Mitchell Institute for Fundamental Physics and Astronomy, Department of Physics & Astronomy, Texas A&M University, College Station, TX 77843

³ Max Planck Institute for Astrophysics, Garching, Germany

⁴ Max-Planck-Institut für Extraterrestrische Physik, Garching, Germany

ies leaves some open questions, in particular regarding the importance of survey wavelength and the variation as a function of sample morphology. Thus we wish to clarify the following key issues: How does the bar fraction vary across the late to early type disc galaxies? Does the bar fraction vary with redshift, i.e. do galaxies know they should become barred once they form? Does the bar fraction vary with environment i.e. are bars triggered by gravitational interactions? In order to address the previous questions, we need to anchor the bar fraction at redshift zero: we may be then able to shed light on why some galaxies are barred and others are not.

Thus, the goal of this study is to provide a robust measurement of the bar fraction at $z = 0$, as a function of wavelength, Hubble type, HI mass content and to test and quantify the impact of sample selection on the inferred bar fraction. We quantify the NIR numbers of barred galaxies in the Virgo cluster using newly released observations from the UKIDSS Large Area Survey (H-band imaging). One of the main advantages of the H-band is that it is less sensitive to dust obscuration than B-band imaging typically used for bar studies. We also use HI gas masses from the ongoing ALFALFA survey to study the gas contents of these galaxies. In Paper II of this series we will apply the same approach to a well defined sample of field galaxies for comparison to the cluster sample.

The outline of the present paper is as follows: we present the data in §2, the galaxy classification method in §2.5, our sample selection in §2.4; the results are presented in §3 and discussed in §4. We draw conclusions in §5. Throughout the paper we assume a flat cosmology with $\Omega_M=0.3$, $\Omega_\Lambda=0.7$ and $H_0=75 \text{ km s}^{-1} \text{ Mpc}^{-1}$. We adopt a distance modulus for the Virgo cluster $(m - M) = 30.5$ from de Vaucouleurs (1977) that gives for an angular distance of $1''$ a physical distance of 68 pc.

2. OBSERVATIONS

The Virgo Cluster is the nearest galaxy cluster to the Milky Way and consists of over 2000 known members at a distance of approximately 18 Mpc (Binggeli et al. 1985) and a total mass of about $10^{14} M_\odot$ (Binggeli 1999). Virgo’s extensive substructure indicates it is a dynamically young system; however, Virgo’s proximity makes it an ideal location for investigating the properties of barred galaxies in an over-dense environment. The main challenges in studying galaxies in Virgo are the cluster’s angular size of more than 100 deg^2 and that the typical angular size for individual members is larger than the field-of-view of most CCDs. Thus an extensive and careful observing campaign is needed to identify and obtain accurate photometry for Virgo galaxies.

Fortunately such a catalog already exists in the Virgo Cluster Catalog first presented by Binggeli et al. (1985, VCC hereafter). The VCC is drawn from a long-exposure photographic plate survey covering the range in apparent photographic blue magnitude from $BT^1 = 11$ to 20 (see Binggeli et al. (1984) for details) and the VCC has been the primary source catalog for subsequent studies of the

¹ Throughout our manuscript, BT magnitudes refer to the magnitudes measured by Binggeli et al. (1985) from photographic plates.

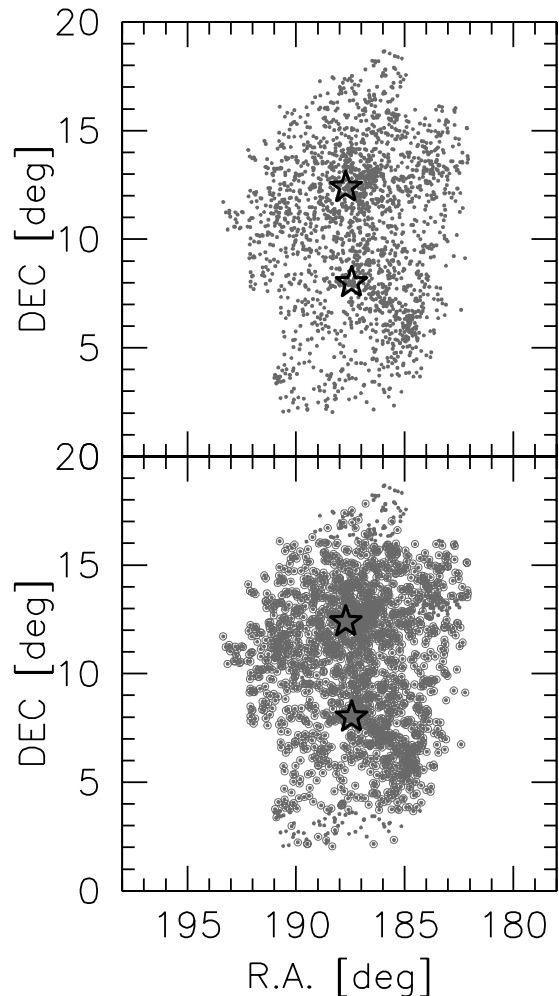


FIG. 1.— *Top*: The spatial distribution of all the VCC+ galaxies on the sky; the two stars are M87 (top) and M49 (bottom). At the distance of M87 (distance modulus of $(m - M) = 30.5$, de Vaucouleurs 1977), 1° corresponds to a physical scale of ~ 0.24 Mpc. *Bottom*: The VCC+ galaxies with H-band imaging from the UKIDSS LAS survey are shown with black circles. The uniform coverage of the NIR imaging confirms that there is no spatial bias in how our samples are selected.

Virgo cluster. We use the VCC as the master catalog throughout our analysis.

While the Virgo members are drawn from the VCC, we capitalize on recently released observations from multiple surveys in our analysis. We focus on three different samples to investigate the bar fraction as a function of:

1. B-band luminosity: Optically selected samples are affected by dust obscuration and are biased towards younger stellar populations. However, we include a B-band selected sample so that we can directly compare to results in the literature and thus quantify the bias between samples selected at different wavelengths.
2. H-band luminosity: NIR selected samples are better tracers of the total stellar mass in galaxies (Bell & de Jong 2001; Balogh et al. 2001) because they are less affected by dust obscuration. Earlier studies (E00) indicate that the bar fraction measured using IR imaging is higher than in the opti-

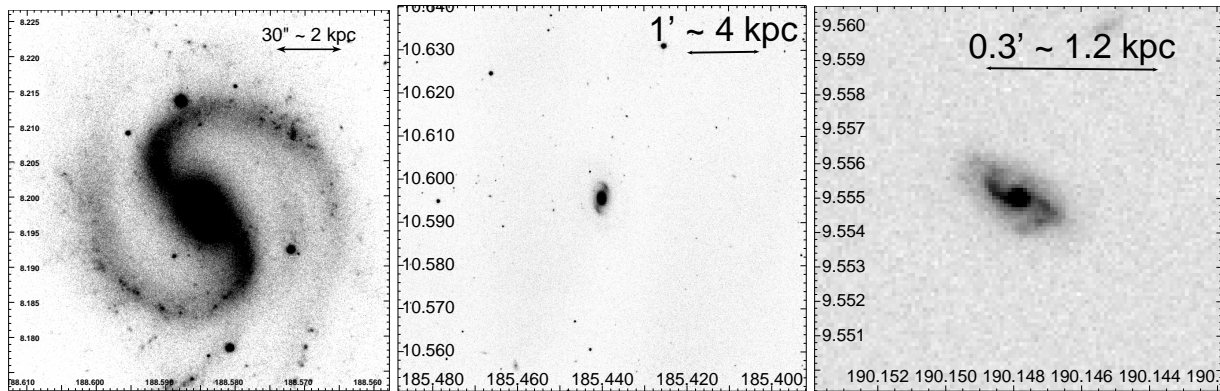


FIG. 2.— UKIDSS LAS H -band images ($0.4''$ /pixel) for VCC 1555, VCC 500 and VCC 1849, three barred galaxies in our analysis that have different projected sizes; the physical scale is shown as a black line in each panel. The high resolution of the H -band imaging enables us to identify bars across the range of luminosity and size spanned by Virgo members and easily includes bars smaller than 1 kpc.

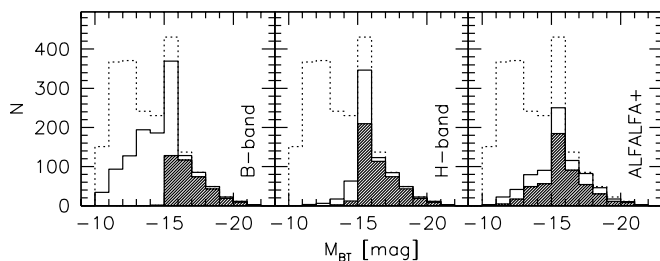


FIG. 3.— The absolute BT magnitude distribution (measured by Binggeli et al. (1985) from photograph plates) for all the VCC+ galaxies (dotted line histograms); note that the VCC+ is complete for galaxies brighter than $M_{BT} \sim -12.5$. The solid-line histograms show the GOLDMine B -band identified members (left), GOLDMine H -band identified members (middle), and ALFALFA+ HI gas mass identified members (right). The shaded histograms in each panel are the members that have NIR imaging from UKIDSS, BH magnitudes from GOLDMine, and ALFALFA+ HI gas masses; we also have excluded highly inclined galaxies (axis ratio < 0.3). The shaded histograms are our defined PRIME samples (see §2.4).

cal.

3. HI gas mass: Selecting by total mass in neutral hydrogen has different selection effects, e.g. HI samples are naturally biased towards gas-rich galaxies that typically have spiral or irregular morphologies (Roberts & Haynes 1994; Gavazzi et al. 2008). If bar formation is strongly coupled to gas mass, we expect to measure a peculiar bar fraction in the HI selected sample.

2.1. Optical Imaging

The GOLDMine database² (Gavazzi et al. 2003) contains multi-wavelength continuum photometry, line photometry, and dynamical and structural parameters for all 2096 Virgo galaxies in the VCC (Binggeli et al. 1985) as well as an additional 60 spectroscopically confirmed members (Gavazzi et al. 1999). We refer to the total database of 2156 Virgo galaxies as VCC+; their spatial distribution is shown in Figure 1 (top panel).

The GOLDMine observations of the VCC were constructed to be optically complete to $BT = 18.0$ ($M_{BT} = -12.5$ using a distance modulus for Virgo of $(m - M) = 30.5$). Imaging and spectroscopic data were collected

over a 15 year period, and the ongoing observing campaign continues to expand the multi-wavelength dataset. From the GOLDmine database we draw coordinates (J2000), Johnson-Cousin BVH Vega magnitudes computed within the optical radius defined by the 25 mag arcsec⁻² isophote (μ_{25} ; Gavazzi & Boselli 1996), the axis ratios (minor to major optical diameter at μ_{25}) and the morphological type (adopted from Binggeli et al. 1985) for the VCC+ galaxies.

2.2. NIR Imaging

The UKIDSS Large Area Survey (LAS)³ (Lawrence et al. 2007) is an ongoing survey to image 4000 deg² at high Galactic latitudes in the $YJHK$ filters to a depth in H of 18.8 mag; for the Virgo cluster, this limiting H -band magnitude corresponds to an absolute magnitude of $M_H \sim -11.7$. The UKIDSS spatial resolution of $0.4''$, average seeing of $0.8''$, and coverage of the Virgo cluster is unprecedented. In comparison, the all-sky 2MASS survey (Skrutskie et al. 2006) imaged the Virgo cluster with a pixel scale of $2''$, has a magnitude limit of $m_H = 14.3$, and is unable to resolve features smaller than ~ 140 pc.

Galaxy bars in the local universe tend to be smaller than 1 kpc (Laine et al. 2002; Barazza et al. 2008); this corresponds to an angular size of $\sim 15''$ at Virgo's distance, a size that is well-sampled by the UKIDSS imaging. Virgo's proximity combined with the UKIDSS resolution means that we can easily resolve bars down to sub-kpc scales. Figure 2 shows UKIDSS H -band imaging for three Virgo galaxies spanning the range in size and includes the smallest barred galaxy in Virgo (diameter $\sim 20''$).

We note that while we use the UKIDSS imaging to identify galaxy bars, we use the H -band magnitudes from GOLDmine for the photometry. The existing UKIDSS data reduction pipeline does not measure the background correctly for very extended sources such as Virgo galaxies, thus the UKIDSS photometry for these objects is

³ UKIDSS uses the UKIRT Wide Field Camera (WFCAM, Casali et al. 2007) and a photometric system described by Hewett et al. (2006). The pipeline processing and science archive are described in Irwin et al. (2010, in prep.) and Hambly et al. (2008). We have used data from the 6th data release: <http://www.ukidss.org/surveys/surveys.html>

² <http://goldmine.mib.infn.it/>

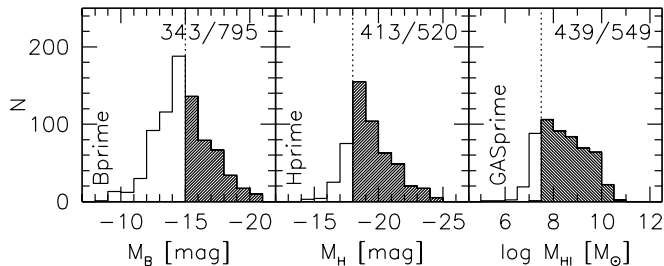


FIG. 4.— We show the GOLDMine B -band magnitude distribution for our BPRIME sample (left), the GOLDMine H -band magnitude distribution for our HPRIME sample (middle), and the ALFALFA+ HI gas mass distribution for our GASPRIME sample (right) as shaded histograms; for explanation of the open histograms, see Figure 3 and §2.4. The dotted vertical lines show the limiting cut for the PRIME samples, i.e. $M_B \leq -15$ mag (left), $M_H \leq -18$ mag (middle), and $M_{HI} \geq 10^{7.5} M_\odot$ (right). The total number of galaxies in each galaxy sample (open histogram) and the number in the PRIME sample (shaded histogram) are included in each panel.

known to be incorrect (Richard McMahon, private communication).

We queried the UKIDSS LAS database for the VCC+ galaxies and retrieved the available H -band stacked frames ($15' \times 90'$). In several cases, the Virgo galaxies are on multiple frames and the frames are stitched together using `swarp` (Bertin et al. 2002). Figure 1 (bottom panel) shows the spatial distribution of the VCC+ galaxies for which we also have H -band imaging from the UKIDSS LAS. The uniform coverage of the H -band imaging compared to the optical indicates that there is no spatial bias in how our samples are selected (see §2.4).

2.3. HI Gas Masses

The Arecibo Legacy Fast ALFA (ALFALFA⁴) (Giovanelli et al. 2005) survey is an on-going blind extragalactic search for neutral hydrogen (HI) that will cover 7074 degrees² of the high galactic latitude sky accessible to the Arecibo telescope, i.e. $03h < \alpha < 22h$ and $0^\circ < \delta < +36^\circ$. The ALFALFA survey covers the entire Virgo Cluster with a spatial accuracy of $\sim 20''$ for the centroids of galaxies, a beam-size of $3.5'$, and an HI-mass detection limit of $M_{HI} \geq 10^{7.5} M_\odot$. For our analysis, we obtain HI masses for all the available VCC+ galaxies from the current ALFALFA data release which covers the Virgo region at $\delta > +8^\circ$ (Giovanelli et al. 2007; Kent et al. 2009).

The GOLDmine database also contains HI data taken with Arecibo, the *Very Large Array*, and the Nançay radio telescope for the VCC+. We integrate these HI observations (Gavazzi et al. 2005) with those from the ALFALFA survey to obtain HI masses for Virgo galaxies at $\delta < +8^\circ$; we refer to the combined HI catalog as ALFALFA+.

2.4. Defining the PRIME Samples

One of our goals is to determine if the galaxy bar fraction depends on how the galaxy samples are defined. In our analysis, we consider only galaxies that are covered by the UKIDSS imaging with measured B (optical) and H (NIR magnitudes from GOLDMine) and HI gas masses. Figure 3 shows the absolute magnitude (M_{BT})

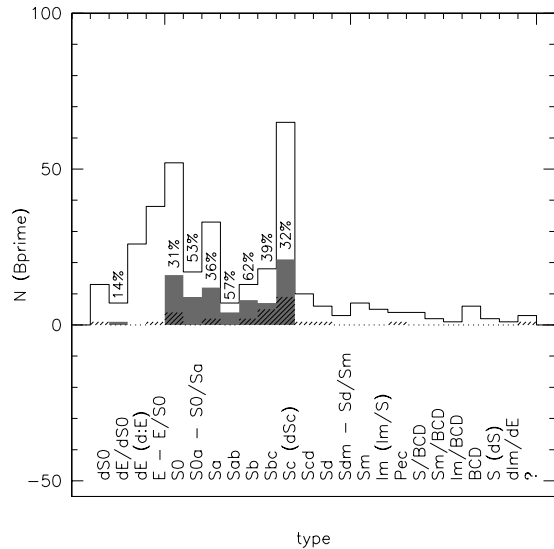


FIG. 5.— The morphological distribution of Virgo members in our BPRIME sample (solid line). The filled histogram represents the galaxies classified as barred using UKIDSS H -band imaging; the barred fraction in each bin is quoted. The hatched histogram represents the galaxies with “uncertain” bar classification; in our analysis, these are grouped with the non-barred members.

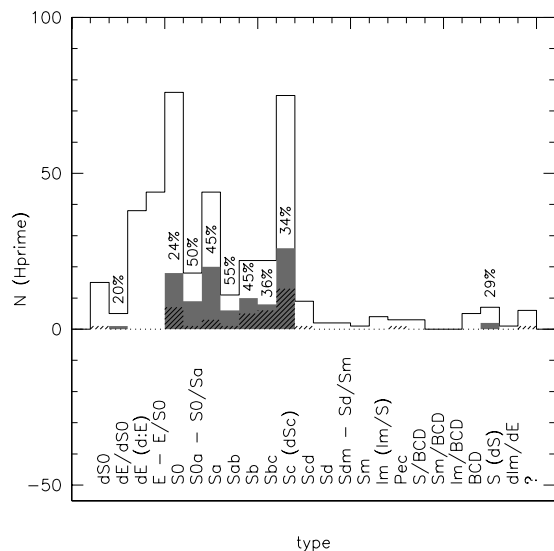


FIG. 6.— Same as in Figure 5 except for our HPRIME sample. Despite selecting in the infrared instead of the optical, the HPRIME sample has essentially the same morphological distribution as the BPRIME sample.

distribution of the VCC+ galaxies (dotted histogram). The solid histograms in the three panels of Figure 3 show the 1) GOLDMine B -magnitude identified members (left), 2) GOLDMine H -magnitude identified members (middle), and 3) HI gas mass identified members (right). The shaded histograms in each panel represent the galaxies used in our analysis; note that our galaxy samples are well-above the VCC+ completeness limit of $M_{BT} \sim -12.5$ (Binggeli et al. 1985).

In our analysis, we exclude highly inclined galaxies (those with axis ratio smaller than 0.3) because edge-on bars are difficult to identify. Lastly, to make up our PRIME samples we use only members brighter than the VCC+ completeness limit of $M_{BT} \sim -12.5$ and we also

⁴ <http://egg.astro.cornell.edu>

TABLE 1
MORPHOLOGICAL COMPOSITION OF THE PRIME SAMPLES^a

	VCC+	BPRIME	HPRIME	GASPRIME
all galaxies	2156	343	413	439
Dwarfs (<i>dE</i> , <i>dS0</i> , <i>dE/S0</i>)	1175 (~55%)	46 (~13%)	58 (~14%)	35 (~8%)
Ellipticals (<i>E-E/S0</i>)	67 (~3%)	38 (~11%)	44 (~11%)	13 (~3%)
Lenticulars (<i>S0-S0/a</i>)	136 (~6%)	69 (~20%)	94 (~23%)	33 (~8%)
Early-type Spirals (<i>Sa-Sb</i>)	128 (~6%)	53 (~16%)	77 (~18%)	53 (~12%)
Late-type Spirals (<i>Sbc-Sm</i>)	236 (~11%)	109 (~32%)	111 (~27%)	150 (~35%)
Irregulars/Peculiars	414 (~19%)	28 (~8%)	29 (~7%)	150 (~34%)

^a Listed is the total number for a given morphological class and its relative fraction to the total number of galaxies (in parentheses).

TABLE 2
BARRED GALAXY FRACTIONS^a

Sample	N	N_{Bar}	Barred %	$N_{Unc.}$	Unc. %
BPRIME – All ^b	343	78	22.7±2.8%	28	8.2±1.6 %
HPRIME – All ^b	413	100	24.2±2.7%	40	9.7±1.6 %
GASPRIME – All ^b	439	75	17.1±2.1%	44	10.0±1.6 %
BPRIME – Discs Only ^c	231	77	33.3±4.4%	24	10.4±2.2%
HPRIME – Discs Only ^c	282	97	34.4±4.0%	37	9.6±2.3%
GASPRIME – Discs Only ^c	241	70	29.0±3.9%	36	14.9±2.7%

^a All bar classifications assigned using UKIDSS H-band imaging. The “uncertain” class contains members for which there was no unanimous agreement on the classification; these make up < 10% in each of the PRIME samples. In our analysis, the uncertain galaxies are included with the non-barred galaxies.

^b The bar fraction relative to all galaxies in the PRIME sample.

^c The bar fraction relative to only the PRIME disc galaxies (*S0-Sm*).

TABLE 3
VIRGO GALAXY CATALOGUE FOR PRIME SAMPLES^a.

Galaxy	BPRIME	HPRIME	GASPRIME	M_B ^b	M_H ^c	M_{HI} ^d	type ^e	class ^f
VCC 3	no	no	yes	-13.50	...	8.67	IRR	no
VCC 4	no	no	yes	-13.13	...	8.25	IRR	no
VCC 6	no	yes	no	-14.81	-18.30	...	ETS	yes
VCC 9	yes	yes	no	-16.23	-19.06	7.45	DWF	no
VCC 12	no	yes	yes	-14.76	-18.64	8.04	ETS	yes
VCC 14	no	no	yes	-13.52	...	9.41	IRR	no
VCC 16	no	no	yes	9.08	LTS	no
VCC 17	no	no	yes	-14.22	-16.20	8.78	IRR	no
VCC 18	yes	yes	yes	-15.20	-18.93	9.99	LTS	no

^a Rest of table available as online material.

^b B-band magnitude from GOLDMine.

^c H-band magnitude from GOLDMine.

^d HI gas mass (in units of $\log M_\odot$) from ALFALFA+.

^e Morphological classification from VCC+: DWF (*dE*, *dS0*, *dE/S0*), ELL (*E-E/S0*), LEN (*S0-S0a*), ETS (*Sa-Sb*), LTS (*Sbc-Sm*), IRR (*Im*, *Pec*, *S/BCD*, *Sm/BCD*, *Im/BCD*, *BCD*, *dS*, *dIm*, ?).

^f Bar classifications assigned using UKIDSS H-band imaging.

apply a luminosity or HI gas mass cut to minimize any potential bias due to incompleteness. Our PRIME samples are:

- BPRIME: Virgo galaxies are selected by their GOLDMine B -band magnitude and we consider only galaxies brighter than $M_B = -15$ mag (343 members); Figure 4 (left) shows the GOLDMine B -band magnitude distribution of this sample. We compare results with the BPRIME sample to results from recent *optically-selected* studies.
- HPRIME: Virgo galaxies are selected by their GOLDMine H -band magnitude and we consider only galaxies brighter than $M_H = -18$ mag (413 members); Figure 4 (middle) shows the GOLDMine H -band magnitude distribution of this sample. Selecting by H -band luminosity should provide a more robust determination of the bar fraction because the H -band is less affected by dust. The BPRIME and HPRIME samples overlap significantly; most of the HPRIME members that are not in the BPRIME sample are spirals with high dust

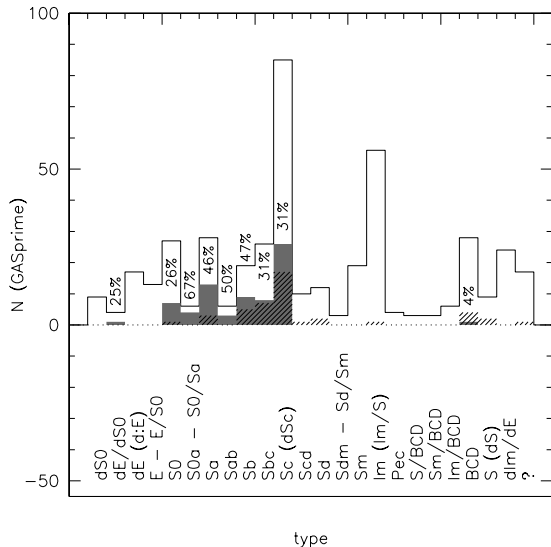


FIG. 7.— Same as in Figure 5 except for our GASPRIME sample. The morphological distribution of the GASPRIME sample is very different from the BPRIME and HPRIME samples: selecting by HI gas mass includes many more late-type spiral and irregular galaxies and significantly fewer elliptical and lenticular galaxies.

content.

- GASPRIME: Virgo galaxies are selected by their ALFALFA+ HI gas mass (neutral hydrogen) and we consider only galaxies with $M_{HI} \geq 10^{7.5} M_{\odot}$ (439 members); Figure 4 (right) shows the HI gas mass distribution of this sample. If HI gas mass is correlated with bar formation, we expect the bar fraction in the GASPRIME sample to be highest.

2.5. Classification Method

As part of our analysis, we use the detailed morphological types from the VCC+. For simplicity, we define six broad morphological classes: dwarfs (dE , $dS0$, $dE/S0$), ellipticals (E , $E/S0$), lenticulars ($S0$, $S0a$; defined as red, featureless discs with very little to no sign of star formation), early spirals (Sa , Sab , Sb ; defined as spiral galaxies with a dominant bulge component), late spirals (Sbc , Sc , Scd , Sd , Sm ; defined as spiral galaxies with small bulges or bulge-less), and irregulars/peculiar/blue compact dwarfs (Im , Pec , S/BCD , Sm/BCD , Im/BCD , BCD , dS , dIm , ?). The morphological make-up of the three PRIME samples is listed in Table 1.

Recognizing that there are multiple approaches on how to identify galaxy bars, we stress that the strength of our analysis lies in our comparisons being internally consistent. We adopt the straight-forward method of visually classifying galaxies into one of three categories: “barred”, “non-barred”, or “uncertain”. Note that the “barred” category includes both strong, elongated bars (SB) to weak oval bars (SAB). Because earlier work by E00 found that the frequency of barred galaxies in the near infrared is nearly twice that measured in the optical, we use the H -band images from UKIDSS to visually identify galaxy bars for all of our PRIME samples.

Three of us (LG, KT, & BM) identified bars by inspecting the UKIDSS H -band imaging for the three PRIME samples; LG and BM repeated the procedure twice with

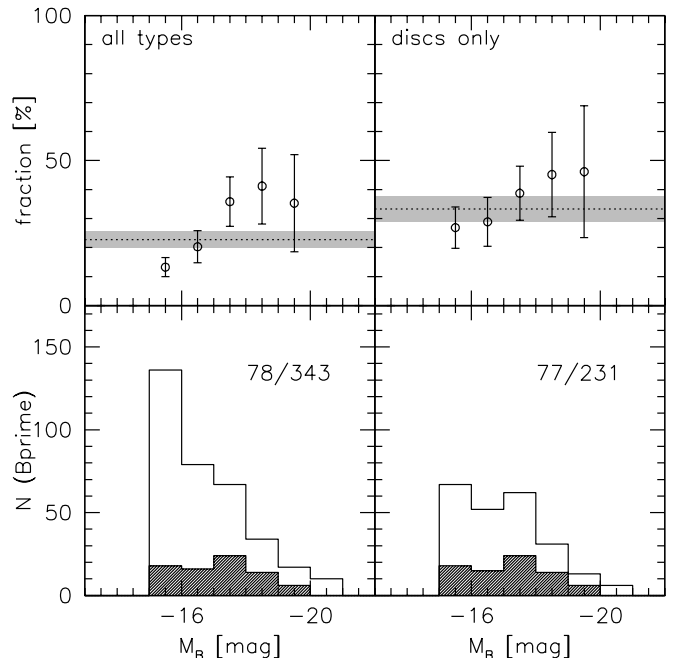


FIG. 8.— *Top panels:* The fraction of barred galaxies in the BPRIME sample as a function of luminosity for all morphological types (left) and only disc galaxies ($S0$ – Sm ; right); morphological classifications are from the VCC+. Note that our galaxy sample spans a factor of ~ 100 in luminosity. The dotted line shows the average barred fraction in the BPRIME sample and the gray shaded region the statistical error. The error bars are the statistical Poisson error per bin. *Bottom panels:* Corresponding histograms of the luminosity distribution for all morphological types (left) and discs only (right); the shaded histograms show the barred members. Included in these panels are the number of barred and total galaxies in the sample. There is a break in the barred fraction for the total BPRIME sample at $M_B \sim -17$ mag where the barred fraction is lower for fainter galaxies; however, the break is weaker in the BPRIME disc only sample. We find that the marginally detected trend of decreasing barred fraction with decreasing luminosity is due to the numerous population of faint dwarf galaxies ($M_B \gtrsim -16$ mag) of which $< 1\%$ are barred (see also Figure 5).

a general agreement of $\sim 92\%$. If there was unanimous agreement, we adopted the classification. If not, the classification was “uncertain”; note that fewer than 10% of PRIME galaxies have “uncertain” bar classifications (see Table 2). In the following analysis, we group the “uncertain” galaxies with the non-barred ones. Table 3 lists the photometry, HI gas mass, morphological type, and bar classification for the Virgo galaxies in our PRIME samples.

Figures 5, 6, & 7 show the morphological distributions of the BPRIME, HPRIME, and GASPRIME samples respectively, and we include the barred, non-barred, and uncertain classifications as assigned by us. The Virgo cluster does have a number of elliptical galaxies (Table 1); however, the majority of members are lenticular and spiral galaxies. In our analysis, we group $S0$ to Sm galaxies together as disc members (e.g. in Table 2). Note that the morphological distribution of the BPRIME and HPRIME samples are very similar, but that the GASPRIME sample includes many more late-type spiral and irregular galaxies and significantly fewer elliptical and lenticular galaxies.

3. RESULTS

In this section we present how the barred galaxy fraction depends on selection method in our PRIME samples.

TABLE 4
 BARRED FRACTION^a AS A FUNCTION OF LUMINOSITY & HI MASS

All Galaxies	BPRIME ^b		HPRIME ^c		GASPRIME ^d	
	M_B	Barred %	M_H	Barred %	M_{HI}	Barred %
	-15 mag	22.7%	-18 mag	24.3%	$10^{7.5} M_\odot$	17.1%
	-16 mag	29.0%	-19 mag	27.5%	$10^{8.5} M_\odot$	25.1%
	-17 mag	34.4%	-20 mag	33.1%	$10^{9.5} M_\odot$	26.1%
Discs Only	M_B	Barred %	M_H	Barred %	M_{HI}	Barred %
	-15 mag	34.8%	-18 mag	34.8%	$10^{7.5} M_\odot$	32.0%
	-16 mag	36.6%	-19 mag	36.8%	$10^{8.5} M_\odot$	34.7%
	-17 mag	39.6%	-20 mag	40.5%	$10^{9.5} M_\odot$	33.8%

^a All bar classifications assigned using UKIDSS H-band imaging.

^b Barred Fraction when considering only BPRIME galaxies brighter than this magnitude limit.

^c Barred Fraction when considering only HPRIME galaxies brighter than this magnitude limit.

^d Barred Fraction when considering only GASPRIME galaxies with HI masses greater than this limit.

TABLE 5
 BARRED GALAXY FRACTION: RED SEQUENCE VS. BLUE CLOUD^a

Sample	$N(\text{RS}^b)$	$N_{\text{Bar}}(\text{RS}^b)$	Barred % (RS ^b)	$N(\text{BC}^c)$	$N_{\text{Bar}}(\text{BC}^c)$	Barred % (BC ^c)
BPRIME – All ^d	230	59	25.7±3.7%	91	19	20.9±5.3%
HPRIME – All ^d	298	74	24.8±3.2%	84	19	22.6±5.6%
GASPRIME – All ^d	161	46	28.6±4.8%	108	20	18.5±4.5%

^a All bar classifications assigned using UKIDSS H-band imaging.

^b Galaxies on the Red Sequence (RS) as defined by the CM relation (§3.3).

^c Galaxies in the Blue Cloud (BC) as defined by the CM relation (§3.3).

^d The bar statistics in the Red Sequence or Blue Cloud using all morphological types in the PRIME sample.

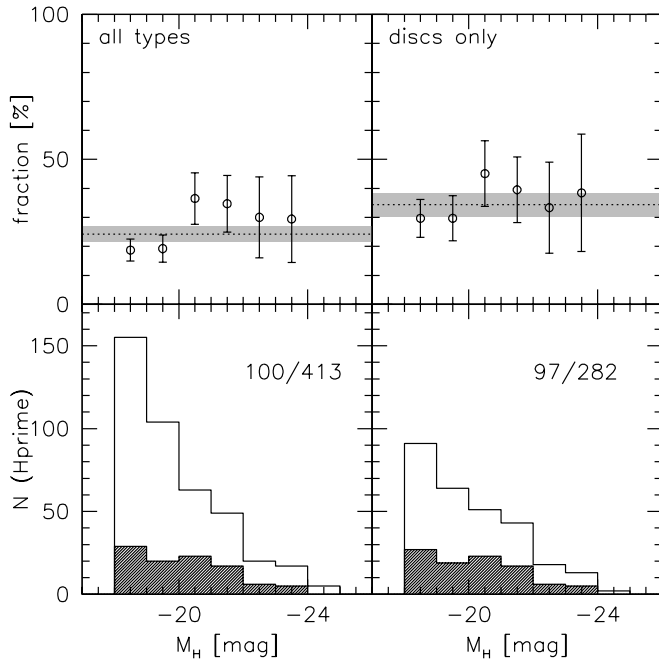


FIG. 9.— Same as Figure 8 but for the HPRIME sample. As in the BPRIME sample, the barred fraction is lower in the two faintest luminosity bins ($M_H > -20$) but fairly constant at higher luminosities. Because the change in barred fraction with luminosity is more evident in the total HPRIME sample, it supports our conclusion that the lower barred fraction at fainter luminosities is due to the numerous population of faint dwarf galaxies.

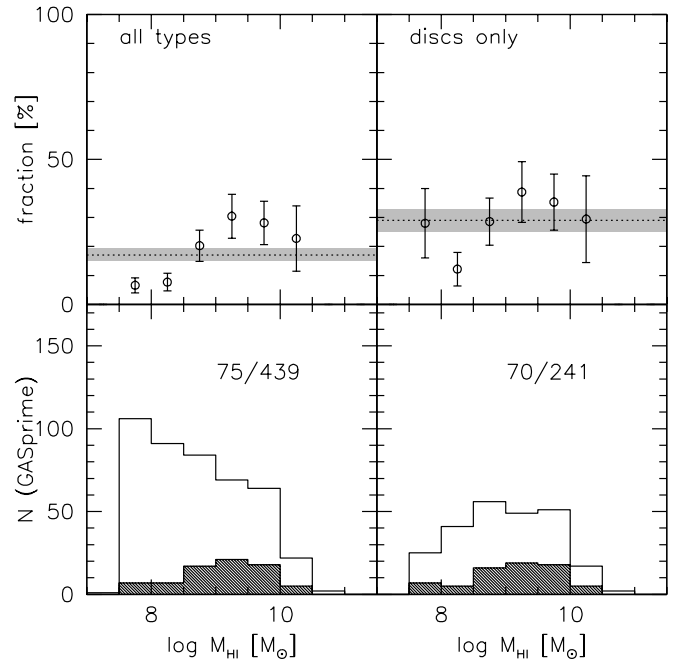


FIG. 10.— Same as Figs. 8 & 9 but for the GASPRIME sample. Similar to results in the BPRIME and HPRIME samples, the barred fraction is lowest for the galaxies with the smallest HI gas masses ($< 10^{8.5} M_\odot$) and fairly constant for galaxies with more HI. The lower barred fraction at lower HI gas mass is due to the numerous population of dwarf galaxies, in particular the irregular galaxies in the GASPRIME sample.

We compare barred fractions for all and disc-only populations as defined by morphology and color. In our analysis, we calculate Poissonian statistical errors following Gehrels (1986).

3.1. Barred Fraction: All Galaxies vs. Discs Only

If we consider all galaxies in the PRIME samples, we find that the barred fraction ranges from 17% (GASPRIME, Table 2) to 24% (HPRIME). The similar barred fractions are surprising given the different morphological compositions of the PRIME samples: only $\sim 50\%$ of galaxies in the GASPRIME sample are classified as discs ($S0-Sm$) compared to $\sim 67\%$ in both the BPRIME and HPRIME samples (see Table 1). Note that regardless of selection method, virtually all of the barred galaxies have morphological type $S0-Sm$.

The barred fraction is traditionally defined as the number of barred discs over the total number of disc galaxies, and the most common method for excluding non-disc galaxies is to use morphological information. We consider only the morphologically-selected disc galaxies defined as having Hubble type $S0$ to Sm , i.e. galaxies with a clearly defined disc component. The barred fraction for disc galaxies is lowest in the GASPRIME sample ($\sim 29\%$) and highest in the HPRIME sample ($\sim 34\%$). However, the barred fraction does not vary strongly across the PRIME samples even when considering only disc galaxies (Table 2).

We find that the barred galaxy fraction in Virgo remains remarkably similar across the three PRIME samples both when considering only disc galaxies and when including all morphological types (Table 2): the traditionally defined barred fraction (discs only) is $\sim 30\%$ while the total barred fraction (all morphological types) is $\sim 20\%$. We find that the barred fraction for discs in the Virgo cluster is only about half that measured by E00 in their heterogeneous sample of discs.

3.2. Barred Fraction vs. Luminosity

The galaxies in our PRIME samples span a wide range in luminosity (factor of ~ 100), thus we can test whether the barred galaxy fraction varies with luminosity. In the BPRIME sample, there is a break at $M_B \sim -17$ such that the barred fraction is lower for fainter systems (Figure 8); the break is most evident when considering all morphological types. If we apply magnitude cuts to the BPRIME sample (Table 4), we find that the barred fraction (all galaxies) increases from 23% ($M_B < -15$ mag) to 34% ($M_B < -17$ mag). At brighter luminosities, the barred fraction remains constant. The break is weaker when considering only BPRIME discs (increases from 35% to 40%; Table 4).

We note that dwarf and irregular galaxies can have bar signatures (Barazza et al. 2002; Lisker et al. 2007) due to, e.g. morphological transformation of discs into dwarf ellipticals and spheroids by the cluster potential (Moore et al. 1996; Mastropietro et al. 2005). However, the barred fraction for these low-mass galaxies is significantly lower: Lisker et al. (2007) find that $< 10\%$ (37/413) have signatures of bars. Among the galaxies in our PRIME samples, we do have a number of dwarf and irregular galaxies (see Figures 5, 6, 7).

In the BPRIME sample, we find that the lower barred fraction at fainter luminosities is due to the population of

dwarf galaxies; these are excluded when considering only discs which explains the weaker break observed in the disc-only sample (Figure 8; Table 4). The dwarf galaxy population is numerous (it makes $\sim 13\%$ of the BPRIME sample) but has a very low barred fraction: only two of the dwarf galaxies have bars (see Figure 5).

We find the same results in the HPRIME sample for both the total and disc-only samples (Figure 9; Table 4): there is a break at $M_H \sim -20$ where the barred fraction at fainter luminosities is lower, and the barred fraction is higher and remains fairly constant at brighter luminosities. As noted earlier, most of the HPRIME sample overlaps with the BPRIME sample, thus the lower barred fraction at lower luminosities is due to a similar dwarf galaxy population (see Figure 6).

The barred fraction in the GASPRIME sample also decreases significantly at low HI gas masses (Figure 10). This is surprising given the different morphological make-up of the GASPRIME sample compared to the luminosity-selected BPRIME and HPRIME samples (compare Figure 7 to Figures 5 & 6): the GASPRIME sample has a measurably higher fraction of irregular galaxies and lower fraction of lenticulars (see Table 1). However, when considering only disc galaxies, the barred fraction in the GASPRIME sample behaves as in the BPRIME and HPRIME samples, i.e. it does not vary significantly with luminosity.

In summary, all of the PRIME samples show a decrease in the barred fraction with decreasing luminosity or HI gas mass because the barred fraction in non-disc, low-mass galaxies is lower. In the case of the luminosity-selected samples (BPRIME & HPRIME), the lower barred fraction is due to the numerous dwarf population while in the HI gas-mass sample (GASPRIME), it is due to the irregulars. If only disc galaxies are considered, the barred fraction is relatively constant over the luminosity and HI gas mass ranges of our PRIME samples.

3.3. Color-Magnitude Diagram

To investigate the color distribution of barred versus non-barred Virgo members, we first determine the color-magnitude (CM) relation using BH photometry. We fit a least-squares to the CM relation using a merged PRIME catalog and iteratively clip galaxies with a color deviation $\Delta(B-H)$ larger than $(2\sigma_{MAD})^5$. We measure a CM relation of:

$$(B-H) = -0.002M_H + 3.855 \quad (1)$$

with $\sigma_{MAD} \sim 0.35^6$. Galaxies are divided into a red sequence and a blue cloud by measuring each galaxy's color deviation $\Delta(B-H)$ from the fitted CM relation and applying a color-cut of $2\sigma_{MAD}$. Figures 11, 12, & 13 show the color-magnitude diagrams for our three PRIME samples with the fitted CM relation as well as the $\Delta(B-H)$ distributions for the total and barred galaxy populations.

⁵ In case of heavy-tailed distributions, the most robust way of fitting the red-sequence is using the Median Absolute Deviation (MAD) as a scale indicator and using the MAD's relative σ (Beers et al. 1990)

⁶ Note that the GOLDMine photometry is not corrected for reddening across the Virgo field, thus the CM relation that we measured is only valid for internal comparison between our PRIME samples.

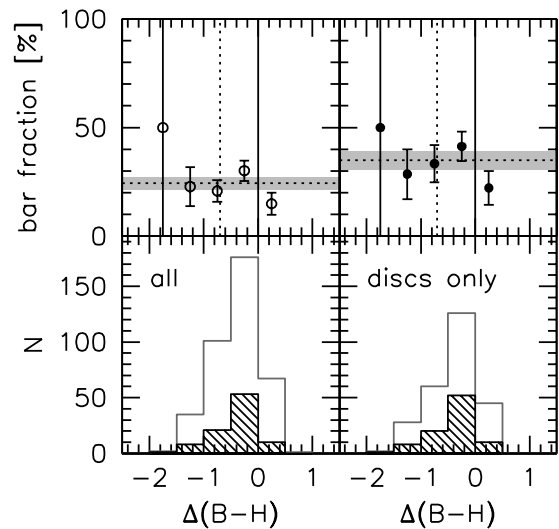
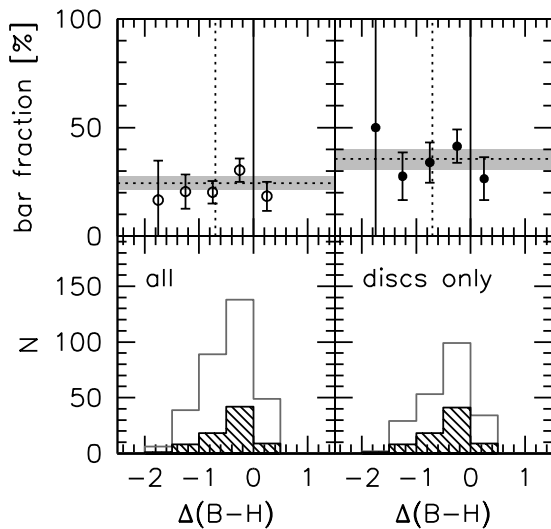
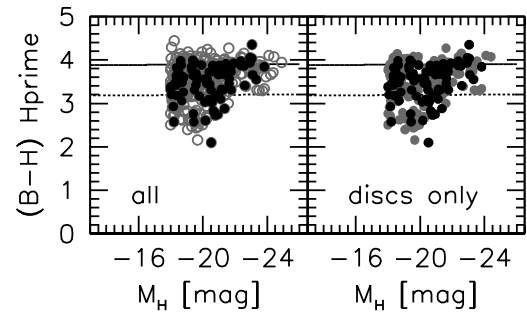
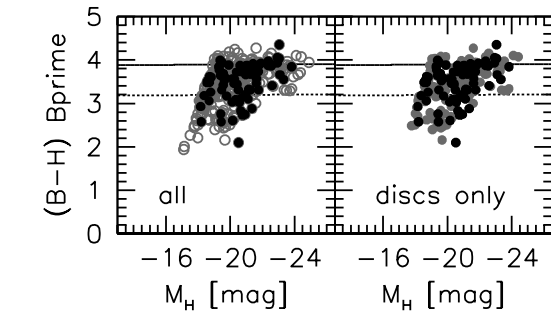


FIG. 11.— *Top*: Color-magnitude (CM) distribution of the galaxies in the BPRIME sample for all morphological types (left) and for discs only (right); open symbols are all galaxies and filled symbols are the barred galaxies. The solid line is the CM relation fit to the merged PRIME sample and the dotted line denotes $2\sigma_{MAD}$ (see §3.3 for details); we use the latter to separate red sequence and blue cloud galaxies. *Bottom*: Distribution of the color deviation $\Delta(B-H)$ from the CM relation for all members (left) and discs only (right); the open histograms are all galaxies and the shaded histograms the barred galaxies. The sub-panels show the barred fraction as a function of $\Delta(B-H)$; the solid vertical line denotes no color deviation and the dotted vertical line denotes the separation between red sequence and blue cloud members ($2\sigma_{MAD}$). The barred galaxies have the same color distribution as the total BPRIME population.

FIG. 12.— Same as Figure 11 but for the HPRIME sample. Again, we find that the barred galaxies have the same color distribution as the total population.

If blue (disc-dominated) spirals have a higher barred fraction (Barazza et al. 2008), barred galaxies on average should then have bluer colors. However, we find that the barred galaxies have the same color distribution as the total galaxy population in both BPRIME and HPRIME samples. This is true when considering all morphological types (Figures 11 & 12, left panels) as well as only disc members (right panels). The barred fraction also stays essentially constant as a function of $\Delta(B-H)$, i.e. the barred fraction is not significantly higher in the blue cloud (Table 5).

In contrast, the barred fraction in the GASPRIME sample does depend on color: when considering all morphological types (Figure 13, left panels), the significant number of gas-rich irregular galaxies ($\sim 1/3$ of the entire sample; see §3.2, Figure 7, and Table 1) populating the

faint blue region of the CM diagram results in a lower barred fraction for bluer galaxies. We find that the irregular galaxies in the GASPRIME sample all lie in the blue cloud and that less than 1% are barred including the irregulars causes the global barred fraction to drop from $\sim 29\%$ on the red sequence to $\sim 19\%$ in the blue cloud (Table 5).

Although both the BPRIME and HPRIME samples have dwarf galaxies that also have a low barred fraction (see §3.2), the dwarf galaxies span a range in color and include red sequence members while the irregulars in the GASPRIME sample are all blue. When only disc members are considered, i.e. when dwarf and irregular galaxies are excluded, the barred fraction in the GASPRIME sample behaves as in the BPRIME and HPRIME disc-only samples (Figure 13, right panels).

In summary, the barred fraction in the luminosity-selected samples (BPRIME & HPRIME) has the same color distribution as the total population, and the barred fraction does not vary with color. The barred fraction of $\sim 21 - 26\%$ (Table 5) on both the red sequence and the blue cloud is the same as the value measured for the total galaxy population ($\sim 23\%$; Table 2), i.e. using color as a proxy for morphology and measuring the barred fraction in the blue cloud results in lower barred fraction than that measured using morphologically classified discs

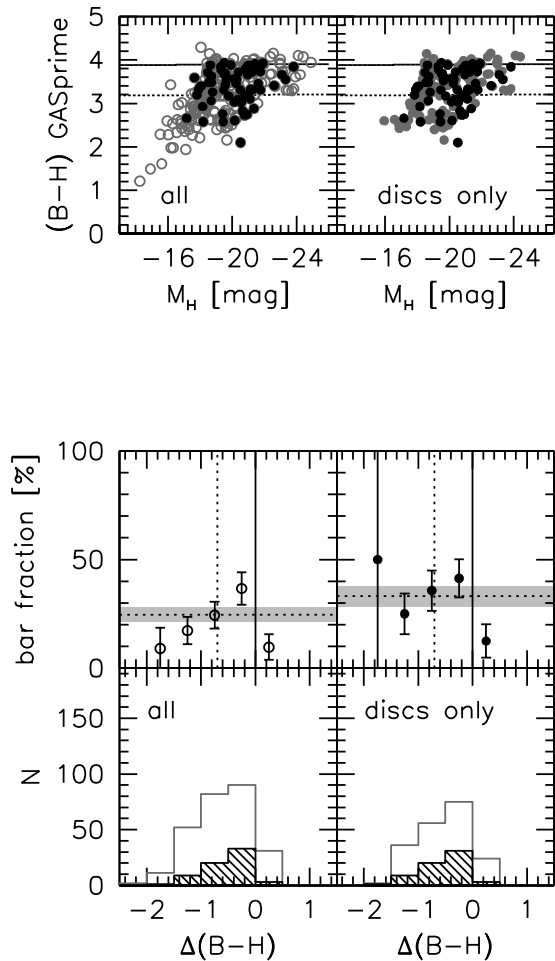


FIG. 13.— Same as Figures 11 & 12 but for the GASPRIME sample. There are many more gas-rich irregular galaxies that populate the faint blue region of the CM diagram. Most of these irregular galaxies are not barred which means that the barred fraction decreases when considering the bluest galaxies in the GASPRIME sample (left panels). However, this effect disappears when only discs ($S0-Sm$) are considered (right panels).

($\sim 34\%$; Table 2). The only color dependence is in the GASPRIME sample where the sample’s significant number of irregular galaxies means that the barred fraction is lower at bluer colors, i.e. in the blue cloud.

3.4. Properties of Barred Lenticular & Spiral Galaxies

Our analysis thus far highlights the importance of including morphology (discs vs. non-discs) to identify trends in the barred population. To further test for any trends in the disc population, we divide our disc samples into lenticular ($S0-S0/a$), early-type spirals ($Sa-Sb$), and late-type spirals ($Sbc-Sm$). We find that the barred fraction is uniformly highest in the early-type spirals (Table 6 & Figure 14): nearly half of the early-type spirals (ETS) are barred compared to less than one third of late-type spirals (LTS).

We test the robustness of this result by generating 10^4 fake datasets using the BPRIME disc sample, keeping the bar fraction fixed as well as the ratio between the three different morphological subclasses (i.e., lenticulars, early- and late-type spirals). For each realization, we randomly pair a 1) disc galaxy and 2) bar/non-bar classification

from the BPRIME disc sample; each realization contains N_D galaxies, where N_D is the total number of BPRIME discs. Only $\sim 0.3\%$ realizations have a barred early-type spiral fraction of $(BF)_{ETS} \geq 45.3\%$ and a barred late-type spiral fraction of $(BF)_{LTS} \leq 25.7\%$, i.e. the observed difference in the barred fractions between early- and late-type spirals (Table 6) is significant at the 3σ level.

Repeating this exercise for the HPRIME and GASPRIME disc samples confirms that the early-type spirals have a higher barred fraction compared to the late-type spirals (3σ significance). Our statistical analysis supports the general conclusion that the barred fraction is highest in early-type spirals in all three PRIME samples and that it is different from the barred fraction in late-type spirals.

With the CM relation, we can also test whether the early-type spirals differ in color from the lenticulars and late-type spirals; the average $(B-H)$ color for each disc population is listed in Table 6. Not surprisingly, the lenticulars mostly lie on the red sequence defined by the fitted CM relation. However, we find that the early-type spirals are nearly as red as the lenticulars while the late-type spirals are significantly bluer; this is true in all of the PRIME samples (Table 6). In general, the early-type spirals in Virgo are more likely to be barred and are redder than late-type spirals. We note that Masters et al. (2009) also find that red spirals tend to be more barred than blue spirals using Galaxy Zoo, a survey that spans a wide range in environment at $z < 0.085$ (Raddick et al. 2007).

Our results differ from Barazza et al. (2008) who find that the barred fraction increases from $\sim 40\%$ in galaxies with prominent bulges to $\sim 70\%$ in disc-dominated galaxies. However, the authors separate bulge and disc-dominated galaxies parametrically by using, e.g. color and/or Sérsic index, and we have shown that the barred fraction measured in a color-selected sample differs from that of a morphologically defined sample (see §3.3). The differences in barred fraction may also be due to using ellipse-fitting in r -band images to identify bars (Barazza et al. 2008) versus visual identification with H-band imaging (this work). Note that the Barazza et al. (2008) sample contains mostly field galaxies while we focus here on the richer environment of Virgo; we explore the environment issue in Paper II of this series.

4. DISCUSSION

4.1. Dependence on Galaxy Morphology

Our study of barred galaxies in the Virgo cluster explores in detail how the barred fraction varies over a wide range in luminosity, HI gas mass, morphology, and color. Using UKIDSS H-band imaging to identify bars, we find that the barred fraction depends most strongly on the morphological composition of the sample: for disc galaxies, the barred fraction is $29 - 34\%$ in both the luminosity-selected samples (BPRIME, HPRIME) and the HI gas mass selected sample (GASPRIME; Table 2). The disc barred fraction does not vary strongly with luminosity nor HI gas mass (Table 4; Figures 8, 9, & 10).

However, the barred fraction in our PRIME samples drops to $17 - 24\%$ when we include all morphological types. The lower barred fractions are due to 1) the ellipticals that make up $\sim 3 - 11\%$ of the PRIME samples and

TABLE 6
DISC GALAXIES: BARRED FRACTIONS^a AND COLORS

Sample	N	N_{Bar}	Barred %	$\mu_{1/2}(B-H)^b$
BPRIME ($S0-Sm$)	231	77	33.3± 4.4%	3.54
BPRIME ($S0-S0/a$) ^c	69	25	36.2± 8.5%	3.79
BPRIME ($Sa-Sb$) ^d	53	24	45.3±11.1%	3.71
BPRIME ($Sbc-Sm$) ^e	109	28	25.7± 5.4%	3.16
HPRIME ($S0-Sm$)	282	97	34.4± 4.0%	3.57
HPRIME ($S0-S0/a$) ^c	94	27	28.7± 6.3%	3.80
HPRIME ($Sa-Sb$) ^d	77	36	46.8± 9.4%	3.71
HPRIME ($Sbc-Sm$) ^e	111	34	30.6± 6.0%	3.18
GASPRIME ($S0-Sm$)	241	70	29.0± 3.9%	3.41
GASPRIME ($S0-S0/a$) ^c	33	11	33.3±11.6%	3.87
GASPRIME ($Sa-Sb$) ^d	53	25	47.2±11.4%	3.72
GASPRIME ($Sbc-Sm$) ^e	155	34	21.9± 4.2%	3.13

^a All bar classifications assigned using UKIDSS H-band imaging.

^b The median ($B-H$) color for these galaxies.

^c Lenticulars.

^d Early-type spirals.

^e Late-type spirals.

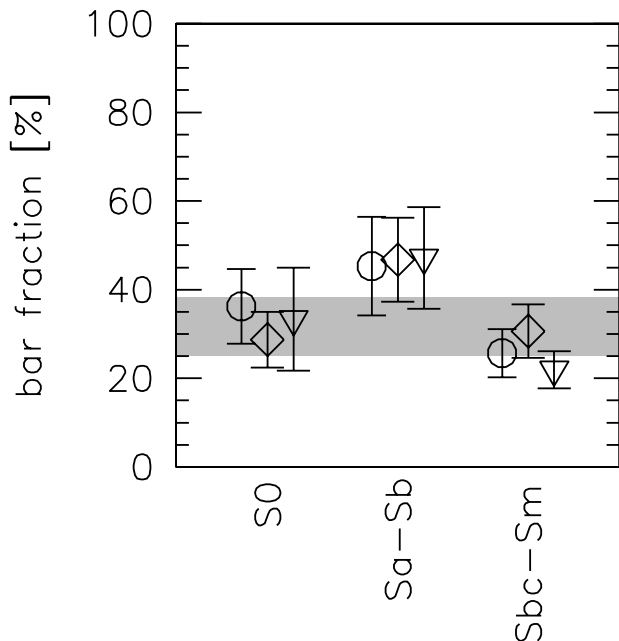


FIG. 14.— Barred fraction for all disc galaxies divided into morphological subclasses: lenticulars ($S0-S0/a$), early-type spirals ($Sa-Sb$) and late-type spirals ($Sbc-Sm$). The BPRIME sample is shown as circles, the HPRIME sample as diamonds, and the GASPRIME sample as triangles; points are slightly offset horizontally for clarity, and statistical Poisson error-bars are included. The shaded horizontal region represents the range in barred fraction of the PRIME disc-only populations. In all three PRIME samples, the early-type spirals have a measurably higher barred fraction relative to the lenticulars and late-type spirals; from statistical tests, we confirm that this result is significant at the 3σ level (see §3.4).

2) the dwarf and irregular galaxies that make up 8–34% of the PRIME samples (Table 1). In Virgo, we find that less than 2% of the dwarf galaxies are barred, and none of the irregular galaxies are barred. Because our study spans a wide range in luminosity and HI gas mass, a large number of these low mass systems are included in our samples, and essentially none of these systems have bars.

The impact of these low mass galaxies can be seen

when comparing the barred fraction versus luminosity or HI gas: there is a break in the barred fraction at lower luminosities (Figures 8 & 9) and HI gas mass (Figure 10). This effect is particularly strong in the GASPRIME sample because there are as many irregular galaxies as late-type spirals (Figure 7).

The inclusion of low mass galaxies will also lower the barred fraction in color-selected samples. If we use color alone to select late-type galaxies, the sample will naturally include a number of irregular galaxies (e.g. Figure 13). The measured barred fraction in blue, presumably disc-dominated systems therefore will be lower than the barred fraction for a morphologically selected disc sample.

A surprising result of our study is that we do not find as high a barred fraction for disc galaxies as E00 ($\sim 70\%$) even though both studies use NIR imaging; the highest barred fraction measured in our PRIME samples is for the early-type spirals ($\sim 45-50\%$). However, most of the 186 galaxies in the E00 sample are luminous ($L > L^*$) discs in the field while our PRIME samples span a wide range in luminosity (factor of ~ 100) and HI gas mass, and we focus only on Virgo members. A more extensive analysis of the barred fraction as a function of environment is in Paper II of this series.

4.2. Barred Fractions of Disc Galaxies

To better understand what physical mechanism sets the barred fraction, we examine how the barred fraction varies in the disc population; note that $> 93\%$ of the bars are in disc galaxies (Table 2). We find that in all three PRIME samples, the early-type spirals have the highest barred fraction ($\sim 45-50\%$) while both the lenticulars and late-type spirals have lower barred fractions (22–36%; Table 6 & Figure 14). The barred early-type spirals are also nearly as red as the barred lenticular galaxies, and both are measurably redder than the barred late-type spirals (Table 6), i.e. barred galaxies are not preferentially bluer than non-barred galaxies.

The difference in barred fraction across the disc population is surprising because in numerical simulations bars are 1) easily triggered through gravitational in-

interactions with other galaxies (Toth & Ostriker 1992; Benson et al. 2004; Dubinski et al. 2008) and 2) difficult to destroy even as the galaxy builds up its central mass (Shen & Sellwood 2004; Athanassoula et al. 2005; Debattista et al. 2006). Thus the barred fraction should not depend on the bulge component.

However, the barred fraction may be higher in early-type spirals due to their higher baryon fractions compared to late-type spirals. The susceptibility of galactic discs to global non-axisymmetric instabilities is the X parameter (Goldreich & Tremaine 1978; Toomre 1981), which for $m = 2$ bar instabilities is:

$$X = \frac{\kappa^2 R}{4\pi G \Sigma} \quad (2)$$

where κ is the epicyclic frequency, R is the radius and the disc surface density is Σ . The inverse dependence on Σ means that ‘maximum’ or heavy discs such as those in early-type spirals are more likely to undergo a bar instability compared to late-type discs that tend to be less luminous, be in smaller dark matter halos, and have lower baryon fractions (McGaugh et al. 2000).

Environment is also likely to have a role, e.g. gravitational interactions with other galaxies and/or the cluster potential can trigger bar instabilities (Moore et al. 1996) as well as transform late-type spirals into dwarf galaxies via galaxy harassment (Moore et al. 1999; Mastropietro et al. 2005). In this scenario, an in-falling late-type spiral undergoes a bar instability during the initial stage of this transformation, but as its stars are stripped and the remaining stellar component heated by gravitational encounters, the galaxy is no longer a late-type spiral. Late-type spirals would become dwarfs in less than a cluster crossing time which, if true, implies that most of the Sc/Sd galaxies in our Virgo cluster sample have yet to travel deep into the cluster potential.

In contrast, the early-type spirals can survive a cluster crossing because they can respond adiabatically to gravitational encounters and are thus less likely to be transformed into dwarfs. However, their discs are heated and in the process become thicker and less susceptible to bar instabilities (Moore et al. 1999), i.e. the early-type spirals can evolve into lenticulars. Note that the early-type spirals are already as red as the lenticulars, thus their luminosity-weighted ages would be comparable.

5. CONCLUSIONS

We study in detail how the barred galaxy fraction varies as a function of luminosity, morphology, color, and HI gas mass in the Virgo cluster by combining the Virgo Cluster Catalog (Binggeli et al. 1985) with multiple public data-sets including recently released NIR imaging from UKIDSS (Lawrence et al. 2007), HI gas masses from ALFALFA (Giovanelli et al. 2005), and photometry from GOLDMine (Gavazzi et al. 2003). We define three PRIME samples where galaxies are selected by their B-band luminosity (343; BPRIME), H-band luminosity (413; HPRIME), and HI gas mass (439; GASPRIME). Bars are visually assigned using the high resolution H-band imaging from UKIDSS; highly inclined systems are excluded.

For morphologically selected discs, the barred fraction in Virgo is $\sim 29 - 34\%$ in all three of our PRIME samples, i.e. the barred disc fraction does not depend strongly on

how the sample is defined. The barred disc fraction is surprisingly robust: it shows little variation with luminosity or HI gas mass. We also do not find any evidence of barred galaxies being preferentially blue: the barred galaxies have the same $(B - H)$ color distribution as the total PRIME populations.

We find that the barred fraction depends most strongly on morphological composition: when all galaxies in the PRIME samples are included, the barred fraction drops to $\sim 17 - 24\%$. The lower barred fraction relative to discs-only is due to ellipticals as well as numerous dwarf and irregular galaxies that are included because of our wide ranges in luminosity (factor ~ 100) and HI gas mass ($M_{HI} > 10^{7.5} M_{\odot}$). Essentially none of the dwarf and irregular galaxies are barred, but they make up to, e.g. 34% of the GASPRIME sample. These low-mass galaxies cause the barred fraction to decrease at low luminosities/HI gas masses. For studies that use color alone to select blue, presumably disc-dominated galaxies, the dwarf and irregular galaxies will lower the measured barred fraction compared to that for a morphologically selected disc sample.

When the disc populations are separated into lenticulars ($S0-S0/a$), early-type spirals ($Sa-Sb$), and late-type spirals ($Sbc-Sm$), we find that the early-type spirals have a higher barred fraction ($\sim 45 - 50\%$) compared to the lenticulars and late-type spirals ($\sim 22 - 36\%$). Statistical tests confirm that the difference in the barred fractions is significant at the 3σ level. The early-type spirals are as red in $(B - H)$ color as the lenticulars, and both are redder than the late-type spirals.

A possible explanation for the higher barred fraction in early-type spirals and their red colors is that while bars are easily triggered in disc galaxies, only discs with large baryon fractions/bulges survive passage through the cluster potential. The early-type spirals form bars but lose their gas to the intra-cluster medium and so stop forming new stars. Gravitational interactions with other galaxies and the cluster potential eventually heat the disc which then dissolves the bar, and the early-type spiral evolves into a lenticular galaxy. Bars also form in the late-type spirals, but these galaxies are transformed by gravitational encounters into dwarf galaxies in less than a cluster crossing time.

We note that the barred disc fraction in our PRIME samples is half that measured by E00 using NIR imaging of local disc galaxies. However, the E00 sample is dominated by ($L > L^*$) field galaxies while our study focuses on galaxies spanning a range in luminosity in the richer environment of Virgo. To determine if the barred fraction varies with environment, we compare our Virgo results to a field sample in Paper II of this series.

We thank V. Debattista and S. Jogee for helpful discussion. This paper has made use of the GOLD Mine database and of HI measurements collected at the Arecibo Observatory for the ALFALFA survey. The Arecibo Observatory is part of the National Astronomy and Ionosphere Center which is operated by Cornell University under a cooperative agreement with the National Science Foundation. We are grateful for access to the ALFALFA data and acknowledge the leadership of the ALFALFA survey’s Principal Investigators Martha Haynes

and Riccardo Giovanelli, and the valuable contributions of the other ALFALFA team members. L.G., K.T., and

A.S. acknowledge generous support from the Swiss National Science Foundation (grant PP002-110576).

REFERENCES

- Aguerri, J. A. L., Méndez-Abreu, J., & Corsini, E. M. 2009, *A&A*, 495, 491
- Athanassoula, E. 2005, *MNRAS*, 358, 1477
- Athanassoula, E., Lambert, J. C., & Dehnen, W. 2005, *MNRAS*, 363, 496
- Balogh, M. L., Christlein, D., Zabludoff, A. I., & Zaritsky, D. 2001, *ApJ*, 557, 117
- Barazza, F. D., Binggeli, B., & Jerjen, H. 2002, *A&A*, 391, 823
- Barazza, F. D., Jablonka, P., Desai, V., Jogee, S., Aragón-Salamanca, A., De Lucia, G., Saglia, R. P., Halliday, C., Poggianti, B. M., Dalcanton, J. J., Rudnick, G., Milvang-Jensen, B., Noll, S., Simard, L., Clowe, D. I., Pelló, R., White, S. D. M., & Zaritsky, D. 2009, *A&A*, 497, 713
- Barazza, F. D., Jogee, S., & Marinova, I. 2008, *ApJ*, 675, 1194
- Beers, T. C., Flynn, K., & Gebhardt, K. 1990, *AJ*, 100, 32
- Bell, E. F., & de Jong, R. S. 2001, *ApJ*, 550, 212
- Benson, A. J., Lacey, C. G., Frenk, C. S., Baugh, C. M., & Cole, S. 2004, *MNRAS*, 351, 1215
- Bertin, E., Mellier, Y., Radovich, M., Missonnier, G., Didelon, P., & Morin, B. 2002, in *Astronomical Society of the Pacific Conference Series*, Vol. 281, *Astronomical Data Analysis Software and Systems XI*, ed. D. A. Bohlender, D. Durand, & T. H. Handley, 228–+
- Binggeli, B. 1999, in *Lecture Notes in Physics*, Berlin Springer Verlag, Vol. 530, *The Radio Galaxy Messier 87*, ed. H.-J. Röser & K. Meisenheimer, 9–+
- Binggeli, B., Sandage, A., & Tammann, G. A. 1985, *AJ*, 90, 1681
- Binggeli, B., Sandage, A., & Tarengi, M. 1984, *AJ*, 89, 64
- Böker, T., Stanek, R., & van der Marel, R. P. 2003, *AJ*, 125, 1073
- Bureau, M., & Athanassoula, E. 2005, *ApJ*, 626, 159
- Carollo, C. M., Stiavelli, M., de Zeeuw, P. T., & Mack, J. 1997, *AJ*, 114, 2366
- Carollo, C. M., Stiavelli, M., & Mack, J. 1998, *AJ*, 116, 68
- Casali, M., Adamson, A., Alves de Oliveira, C., Almaini, O., Burch, K., Chuter, T., Elliot, J., Folger, M., Foucaud, S., Hambly, N., Hastie, M., Henry, D., Hirst, P., Irwin, M., Ives, D., Lawrence, A., Laidlaw, K., Lee, D., Lewis, J., Lunney, D., McLay, S., Montgomery, D., Pickup, A., Read, M., Rees, N., Robson, I., Sekiguchi, K., Vick, A., Warren, S., & Woodward, B. 2007, *A&A*, 467, 777
- Combes, F., Debbasch, F., Friedli, D., & Pfenniger, D. 1990, *A&A*, 233, 82
- Courteau, S., Andersen, D. R., Bershad, M. A., MacArthur, L. A., & Rix, H.-W. 2003, *ApJ*, 594, 208
- de Vaucouleurs, G. 1977, *Nature*, 266, 126
- de Vaucouleurs, G., de Vaucouleurs, A., Corwin, Jr., H. G., Buta, R. J., Paturel, G., & Fouque, P. 1991, *Third Reference Catalogue of Bright Galaxies* (de Vaucouleurs, G., de Vaucouleurs, A., Corwin, H. G., Jr., Buta, R. J., Paturel, G., & Fouque, P.)
- Debattista, V. P., Mayer, L., Carollo, C. M., Moore, B., Wadsley, J., & Quinn, T. 2006, *ApJ*, 645, 209
- Dubinski, J., Gauthier, J., Widrow, L., & Nickerson, S. 2008, in *Astronomical Society of the Pacific Conference Series*, Vol. 396, *Astronomical Society of the Pacific Conference Series*, ed. J. G. Funes & E. M. Corsini, 321–+
- Eskridge, P. B., Frogel, J. A., Pogge, R. W., Quillen, A. C., Berlind, A. A., Davies, R. L., Depoy, D. L., Gilbert, K. M., Houdashelt, M. L., Kuchinski, L. E., Ramirez, S. V., Sellgren, K., Stutz, A., Terndrup, D. M., & Tiede, G. P. 2002, *VizieR Online Data Catalog*, 214, 30073
- Eskridge, P. B., Frogel, J. A., Pogge, R. W., Quillen, A. C., Davies, R. L., Depoy, D. L., Houdashelt, M. L., Kuchinski, L. E., Ramirez, S. V., Sellgren, K., Terndrup, D. M., & Tiede, G. P. 2000, *AJ*, 119, 536
- Gavazzi, G., & Boselli, A. 1996, *Astrophysical Letters Communications*, 35, 1
- Gavazzi, G., Boselli, A., Donati, A., Franzetti, P., & Scodreggio, M. 2003, *A&A*, 400, 451
- Gavazzi, G., Boselli, A., Scodreggio, M., Pierini, D., & Belsole, E. 1999, *MNRAS*, 304, 595
- Gavazzi, G., Boselli, A., van Driel, W., & O’Neil, K. 2005, *A&A*, 429, 439
- Gavazzi, G., Giovanelli, R., Haynes, M. P., Fabello, S., Fumagalli, M., Kent, B. R., Koopmann, R. A., Brosch, N., Hoffman, G. L., Salzer, J. J., & Boselli, A. 2008, *A&A*, 482, 43
- Gehrels, N. 1986, *ApJ*, 303, 336
- Giovanelli, R., Haynes, M. P., Kent, B. R., Perillat, P., Saintonge, A., Brosch, N., Catinella, B., Hoffman, G. L., Stierwalt, S., Spekkens, K., Lerner, M. S., Masters, K. L., Momjian, E., Rosenberg, J. L., Springob, C. M., Boselli, A., Charmandaris, V., Darling, J. K., Davies, J., Garcia Lambas, D., Gavazzi, G., Giovanardi, C., Hardy, E., Hunt, L. K., Iovino, A., Karachentsev, I. D., Karachentseva, V. E., Koopmann, R. A., Marinoni, C., Minchin, R., Muller, E., Putman, M., Pantoja, C., Salzer, J. J., Scodreggio, M., Skillman, E., Solanes, J. M., Valotto, C., van Driel, W., & van Zee, L. 2005, *AJ*, 130, 2598
- Giovanelli, R., Haynes, M. P., Kent, B. R., Saintonge, A., Stierwalt, S., Altaf, A., Balonek, T., Brosch, N., Brown, S., Catinella, B., Furniss, A., Goldstein, J., Hoffman, G. L., Koopmann, R. A., Kornreich, D. A., Mahmood, B., Martin, A. M., Masters, K. L., Mitschang, A., Momjian, E., Nair, P. H., Rosenberg, J. L., & Walsh, B. 2007, *AJ*, 133, 2569
- Goldreich, P., & Tremaine, S. 1978, *ApJ*, 222, 850
- Hambly, N. C., Collins, R. S., Cross, N. J. G., Mann, R. G., Read, M. A., Sutorius, E. T. W., Bond, I., Bryant, J., Emerson, J. P., Lawrence, A., Rimoldini, L., Stewart, J. M., Williams, P. M., Adamson, A., Hirst, P., Dye, S., & Warren, S. J. 2008, *MNRAS*, 384, 637
- Hewett, P. C., Warren, S. J., Leggett, S. K., & Hodgkin, S. T. 2006, *MNRAS*, 367, 454
- Kalloghlian, A. T., & Kandalian, R. A. 1998, *Astrophysics*, 41, 119
- Kent, B. R., Spekkens, K., Giovanelli, R., Haynes, M. P., Momjian, E., Cortés, J. R., Hardy, E., & West, A. A. 2009, *ApJ*, 691, 1595
- Laine, S., Kenney, J. D. P., Yun, M. S., & Gottesman, S. T. 1999, *ApJ*, 511, 709
- Laine, S., Shlosman, I., Knapen, J. H., & Peletier, R. F. 2002, *ApJ*, 567, 97
- Lawrence, A., Warren, S. J., Almaini, O., Edge, A. C., Hambly, N. C., Jameson, R. F., Lucas, P., Casali, M., Adamson, A., Dye, S., Emerson, J. P., Foucaud, S., Hewett, P., Hirst, P., Hodgkin, S. T., Irwin, M. J., Lodieu, N., McMahon, R. G., Simpson, C., Smail, I., Mortlock, D., & Folger, M. 2007, *MNRAS*, 379, 1599
- Lisker, T., Grebel, E. K., Binggeli, B., & Glatt, K. 2007, *ApJ*, 660, 1186
- Marinova, I., & Jogee, S. 2007, *ApJ*, 659, 1176
- Marinova, I., Jogee, S., Heiderman, A., Barazza, F. D., Gray, M. E., Barden, M., Wolf, C., Peng, C. Y., Bacon, D., Balogh, M., Bell, E. F., Böhm, A., Caldwell, J. A. R., Häußler, B., Heymans, C., Jahnke, K., van Kampen, E., Lane, K., McIntosh, D. H., Meisenheimer, K., Sánchez, S. F., Somerville, R., Taylor, A., Wisotzki, L., & Zheng, X. 2009, *ApJ*, 698, 1639
- Martinez-Valpuesta, I., Shlosman, I., & Heller, C. 2006, *ApJ*, 637, 214
- Martini, P., & Pogge, R. W. 1999, *AJ*, 118, 2646
- Masters, K. L., Mosleh, M., Romer, A. K., Nichol, R. C., Bamford, S. P., Schawinski, K., Lintott, C. J., Andreescu, D., Campbell, H. C., Crowcroft, B., Doyle, I., Edmondson, E. M., Murray, P., Raddick, M. J., Slosar, A., Szalay, A. S., & Vandenberg, J. 2009, *ArXiv e-prints*
- Mastropietro, C., Moore, B., Mayer, L., Debattista, V. P., Piffaretti, R., & Stadel, J. 2005, *MNRAS*, 364, 607
- McGaugh, S. S., Schombert, J. M., Bothun, G. D., & de Blok, W. J. G. 2000, *ApJ*, 533, L99
- Menéndez-Delmestre, K., Sheth, K., Schinnerer, E., Jarrett, T. H., & Scoville, N. Z. 2007, *ApJ*, 657, 790
- Moore, B., Katz, N., Lake, G., Dressler, A., & Oemler, A. 1996, *Nature*, 379, 613
- Moore, B., Lake, G., Quinn, T., & Stadel, J. 1999, *MNRAS*, 304, 465
- Pfenniger, D., & Norman, C. 1990, *ApJ*, 363, 391
- Raddick, J., Lintott, C. J., Schawinski, K., Thomas, D., Nichol, R. C., Andreescu, D., Bamford, S., Land, K. R., Murray, P., Slosar, A., Szalay, A. S., Vandenberg, J., & Galaxy Zoo team. 2007, in *Bulletin of the American Astronomical Society*, Vol. 38, *Bulletin of the American Astronomical Society*, 892–+
- Roberts, M. S., & Haynes, M. P. 1994, *ARA&A*, 32, 115
- Shen, J., & Sellwood, J. A. 2004, *ApJ*, 604, 614
- Skrutskie, M. F., Cutri, R. M., Stiening, R., Weinberg, M. D., Schneider, S., Carpenter, J. M., Beichman, C., Capps, R., Chester, T., Elias, J., Huchra, J., Liebert, J., Lonsdale, C., Monet, D. G., Price, S., Seitzer, P., Jarrett, T., Kirkpatrick, J. D., Gizis, J. E., Howard, E., Evans, T., Fowler, J., Fullmer, L., Hurt, R., Light, R., Kopan, E. L., Marsh, K. A., McCollon, H. L., Tam, R., Van Dyk, S., & Wheelock, S. 2006, *AJ*, 131, 1163

Toomre, A. 1981, in *Structure and Evolution of Normal Galaxies*,
ed. S. M. Fall & D. Lynden-Bell, 111–136

Toth, G., & Ostriker, J. P. 1992, *ApJ*, 389, 5

van den Bergh, S. 2002, *AJ*, 124, 782